Conference Proceedings of the Society for Experimental Mechanics Series

Piyush R. Thakre · Raman P. Singh
Geoffrey Slipher *Editors*

Mechanics of Composite, Hybrid and Multifunctional Materials, Volume 5

Proceedings of the 2018 Annual Conference on Experimental and Applied Mechanics

SEM

Springer

Conference Proceedings of the Society for Experimental Mechanics Series

Series Editor

Kristin B. Zimmerman, Ph.D.
Society for Experimental Mechanics, Inc.,
Bethel, CT, USA

The Conference Proceedings of the Society for Experimental Mechanics Series presents early findings and case studies from a wide range of fundamental and applied work across the broad range of fields that comprise Experimental Mechanics. This Series volume follows the principle tracks or focus topics featured in the Society's Annual Conference & Exposition and will address critical areas of interest to researchers and design engineers working in all areas of Solid Mechanics by presenting early research findings from experimental and computational investigations related to the processing, characterization, and testing of composite, hybrid, and multifunctional materials.

More information about this series at http://www.springer.com/series/8922

Piyush R. Thakre • Raman P. Singh • Geoffrey Slipher
Editors

Mechanics of Composite, Hybrid and Multifunctional Materials, Volume 5

Proceedings of the 2018 Annual Conference on Experimental and Applied Mechanics

Springer

Editors
Piyush R. Thakre
HHB Bldg. 3B161
Dow Chemical Company
Lake Jackson, TX, USA

Geoffrey Slipher
United States Army Research Laboratory
Adelphi, MD, USA

Raman P. Singh
College of Engineering, Architecture & Technology
Oklahoma State University
Stillwater, OK, USA

ISSN 2191-5644 ISSN 2191-5652 (electronic)
Conference Proceedings of the Society for Experimental Mechanics Series
ISBN 978-3-319-95509-4 ISBN 978-3-319-95510-0 (eBook)
https://doi.org/10.1007/978-3-319-95510-0

Library of Congress Control Number: 2018957356

This Springer imprint is published by the registered company Springer Nature Switzerland AG
The registered company address is: Gewerbestrasse 11, 6330 Cham, Switzerland

Preface

Mechanics of Composite, Hybrid, and Multifunctional Materials represents one of the eight volumes of technical papers presented at the 2018 SEM Annual Conference & Exposition on Experimental and Applied Mechanics organized by the Society for Experimental Mechanics and held in Greenville, SC, June 4–7, 2018. The complete proceedings also includes volumes on *Dynamic Behavior of Materials*; *Challenges in Mechanics of Time-Dependent Materials*; *Advancement of Optical Methods & Digital Image Correlation in Experimental Mechanics*; *Mechanics of Biological Systems & Micro-and Nanomechanics*; *Fracture, Fatigue, Failure and Damage Evolution*; *Residual Stress, Thermomechanics & Infrared Imaging, Hybrid Techniques and Inverse Problems*; and *Mechanics of Additive and Advanced Manufacturing.*

The commercial market for composite continues to expand with a wide range of applications from sporting equipment to aerospace vehicles. This growth has been fueled by new material developments, greater understanding of material behaviors, novel design solutions, and improved manufacturing techniques. The broad range of applications and the associated technical challenges require an increasingly multidisciplinary and collaborative approach between the mechanical, chemical, and physical sciences to sustain and enhance the positive impact of composites on the commercial and military sectors.

New materials are being developed from recycled source materials, leading to composites with unique properties and more sustainable sources. Existing materials are also being used in new and critical applications, which requires a deeper understanding of material behaviors and failure mechanisms on multiple length and time scales. In addition, the unique properties of composites present many challenges in manufacturing and in joining with other materials. New testing methods must be developed to characterize the novel composite properties, to evaluate application and product life cycle performance, and to evaluate impacts and merits of new manufacturing methods.

This volume presents early research findings from experimental and computational investigations related to the processing, characterization, and testing of composite, hybrid, and multifunctional materials.

Lake Jackson, TX, USA — Piyush R. Thakre
Stillwater, OK, USA — Raman P. Singh
Adelphi, MD, USA — Geoffrey Slipher

Contents

Chapter 1
Stimulus-Responsive Interfacial Chemistry in CNT/Polymer Nanocomposites

Frank Gardea, Zhongjie Huang, Bryan Glaz, Shashi P. Karna, Xiyuan Cheng, Zhiwei Peng, and YuHuang Wang

Abstract The enhancement of interfacial interactions in carbon nanotube (CNT)/polydimethylsiloxane (PDMS) polymer matrix composites was investigated. The approach taken was to functionalize the CNTs with the photoreactive molecule benzophenone in order to anchor the CNTs to the polymer chains on demand. The anchoring reaction was activated by the use of externally applied UV irradiation. A comparison was done on randomly dispersed and aligned CNTs in order to observe the effect of orientation on interface mechanics and overall enhancement. The effect of interfacial interaction on the mechanical response was determined through analysis of static mechanical experiments, as an increase in interfacial interaction resulted in an observable change in elastic modulus and yield stress. An increase of 22% in elastic modulus was observed in randomly oriented CNTs while an increase of 93% was observed in aligned CNT composites after exposure to UV light. In addition, alignment of CNTs lead to a more discreet yield stress which allowed for a clearer identification of the onset of interfacial failure. This work provides insight into the intelligent design of composites, starting at the nanoscale, to provide desired on-demand macroscale response.

Keywords Nanocomposites · Carbon nanotubes · Photoreactive · Interface · Adhesion

1.1 Introduction

Polymer based composites with nanoscale fillers show promise for enabling multifunctional nanocomposites with unique properties. Possibilities range from enhanced mechanical [1], electrical [2], and thermal [3] properties to functionalities such as self-healing, sensing, and power storage. However, even as advanced manufacturing methods are developed, the promise of unique materials with advanced capabilities has not been fully met. Nanoscale reinforcements have the potential to increase effective composite properties, with this ability highly dependent on the mechanics of the inclusion-polymer interface. The importance of controlling interfacial interactions between a filler and matrix to obtain desired bulk composite properties has been emphasized in literature [4–7]. Due to scale, nanoparticle composites will induce a greater effect via the interface compared to conventional microparticle composites. For example, the reinforcing effect of nanoparticles is dominated by the interfacial shear strength. The overall strength of a composite material is controlled by the filler-matrix interface and not the filler strength. The strength of the composite is directly proportional to the strength of the interface, which directly correlates to the degree of interaction between filler and matrix [1].

There has been substantial variation in reported nanocomposite properties. For example, increases in elastic modulus have been shown to improve significantly by up to 4 times at CNT loadings varying from 0.2 to 2 vol%, while other studies have shown only slight increases [1]. Furthermore, enhanced mechanical damping in CNT/polymer matrix composites has been shown to be sensitive to the interfacial shear strength [8–10]. Thermal conductivity has been shown to increase by up to 1.5 times for concentrations of 3 wt% CNT [11], while others have shown minimal improvements at similar weight fractions due to large interfacial thermal resistance [12]. The variance of reported macro-scale material property improvements shows the importance of controlled interfacial interactions.

F. Gardea (✉) · B. Glaz
Vehicle Technology Directorate, U.S. Army Research Laboratory, Aberdeen Proving Ground, Aberdeen, MD, USA
e-mail: frank.gardea4.civ@mail.mil

Z. Huang · X. Cheng · Z. Peng · Y. Wang
University of Maryland, Department of Chemistry, College Park, MD, USA

S. P. Karna
Weapons and Materials Research Directorate, U.S. Army Research Laboratory, Aberdeen Proving Ground, Aberdeen, MD, USA

P. R. Thakre et al. (eds.), *Mechanics of Composite, Hybrid and Multifunctional Materials, Volume 5*, Conference Proceedings of the Society for Experimental Mechanics Series, https://doi.org/10.1007/978-3-319-95510-0_1

Given the significant effect of the interfacial properties, controlling interfacial interactions will allow for a way to control macroscopic behavior in nanocomposites. One way of controlling the interfacial interaction is through functionalization of the filler, since an attractive interface will decrease the mobility of polymer chains surrounding it and thus increase the interfacial region [5]. Functionalization refers to the attachment of molecules to the surface of the nanoparticle to improve solubility, dispersion, and interfacial interactions [13]. Fabrication of nanocomposites with functionalized nanoparticles usually consists of a multi-step functionalization treatment of the nanoparticles [13–15] before embedding them into a polymer matrix and allowing the functionalization to naturally bond to the matrix without restriction [16–18]. Functional materials featuring tunable interfaces between components are a growing research area due to unique design tunability and resulting combinational properties. The controlled coupling and interaction at nanoscale interfaces could enable the generation of interesting and exceptional optical, electrical, thermal, and mechanical attributes. Thus, the ability to tune the interface properties during fabrication would be desirable for producing nanocomposites optimized to particular applications. Achieving in-situ control of the interface can be accomplished through stimuli-responsive functionalization. For example, dispersion of single-walled CNTs in solvent has been performed by functionalization with stimuli-responsive dispersants, whether the external stimuli is temperature, pH, CO_2, or photo-irradiation [19]. UV irradiation has been used for photopolymers, in which curing of the polymer is achieved by UV stimulus [20]. While UV light has been successful for curing of photopolymers [20], polymer grafting to thin-films [21], and polymer grafting to nanoparticles dispersed in solvent [13], the use of UV light for in-situ control of interfacial interactions in nanoparticle composites has not been reported in literature.

In this study, we investigate the chemistry of interfacial adhesion between a CNT film and a polymer matrix by the use of the photoreactive molecule benzophenone and study the feasibility of controlling the composite mechanical response by exposure to an external UV stimulus. A comparison between randomly oriented and aligned CNT composites was performed in order to determine the effect orientation has on the overall enhancement of mechanical properties. Photo-responsive materials, which can be excited by light to form chemical bonds or modify physical and chemical properties, are very promising for applications in stimuli-responsive systems with remote control.

1.2 Experimental Methods

1.2.1 Functionalization of CNT Films

The diazonium salt was synthesized based on chemistry developed previously [22, 23]. 4-aminobenzophenone (473 mg, 99%, Sigma Aldrich) was mixed with 2 mL of nanopure water and an aqueous solution of tetrafluoroboric acid (1.5 mL, 48 wt%, Sigma Aldrich). Dissolved sodium nitrite (Sigma Aldrich ≥97.0%, 331 mg in 1 mL of nanopure water) was added dropwise to the mixture and allowed to react for 15 min and the diazonium salt collected via filtration. The salt was dried and stored at 4 °C.

Drawable multiwall CNT (MWCNT) forests were synthesized using chemical vapor deposition methods [24, 25] resulting in MWCNTs with a diameter of 50 nm. The forest was drawn continuously into a film of aligned CNTs, as seen in Fig. 1.1b. The drawn films were immersed in an aqueous solution of diazonium salt (1 mg/mL) for 3 days.

HiPco SWCNTs [26] were reacted with the diazonium salt with a 1:1 molar ratio in aqueous solution with 2 wt% sodium dodecyl sulfate (SDS) surfactant for 2 h. Filtration onto a filter paper produced a randomly distributed CNT thin film. The CNT film/filter was transferred to a cured PDMS film and the filter paper dissolved in acetone.

1.2.2 Fabrication and UV Treatment of Layered Composites

PDMS monomer and crosslinker (Sylgard® 184, Dow Corning) were mixed at a 10:1 ratio. After degassing, the polymer was spin-coated at 1000 rpm for 60 s onto glass slides and cured at 90 °C for 2 h. The CNT films (either aligned or randomly dispersed) were placed on top of the polymer film and chemically treated as mentioned previously. After chemical treatment, a second layer of PDMS was spin coated on top of the CNT layer. The composites were then exposed to 365 nm UV light using an Omnicure LX500 system. The UV light was set to 500 mW/cm^2 and the duration of exposure varied between 0 and 5 min. After UV treatment, the PDMS layer was cured at 90 °C for 2 h. The final composite consisted of a PDMS-CNT-PDMS layered structure with an overall thickness of 170 μm with the CNT film positioned at the center of the composite as shown in Fig. 1.1c.

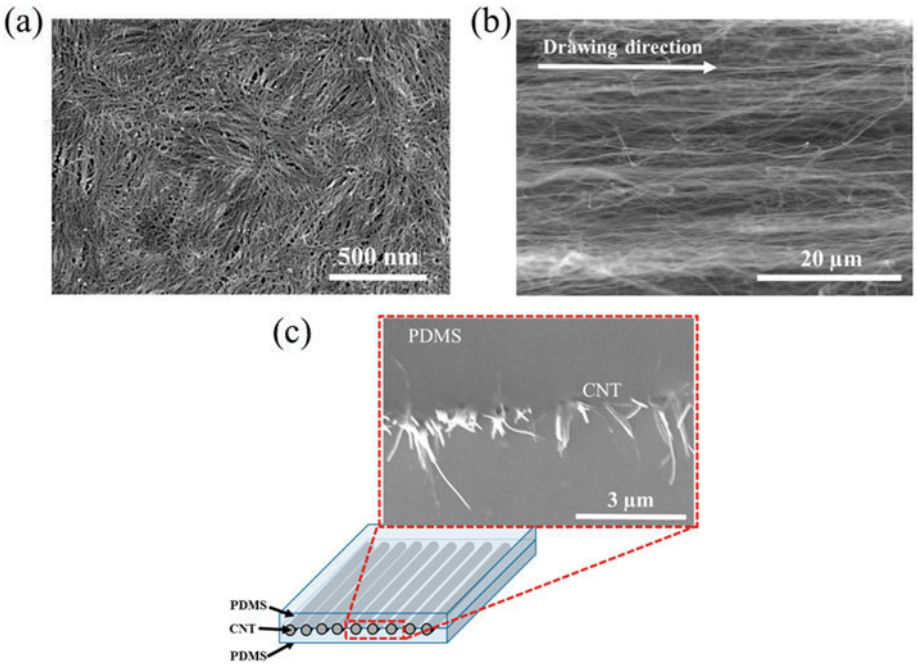

Fig. 1.1 (**a**) SEM image of randomly dispersed SWCNT film (**b**) SEM image of aligned MWCNT film (**c**) Schematic illustrating the composite layered structure. An SEM image of the composite cross-section is shown to verify the layered structure

1.2.3 Experimental Characterization

The degree of functionalization of the CNTs was characterized using Raman spectroscopy [27, 28] using a Horiba Jobin-Yvon LabRam ARAMIS Raman microscope with a 532 nm laser excitation. Absorption spectra was measured using a PerkinElmer Lambda 1050 UV-vis-NIR spectrophotometer. For the film samples, a 150 mm integrating sphere was used. Imaging and observation of CNT arrangement was performed using a Hitachi SU-70 scanning electron microscope (SEM). Static mechanical testing was performed using a Shimadzu-AGS-X series tensile tester. The elastic modulus was obtained from the initial linear portion of the response while the yield stress was taken as the stress value at the onset of nonlinearity determined using a tangent analysis method.

1.3 Results and Discussion

Inspiration from thin-film polymer-grafting technology [21] was obtained to develop a successful nanoparticle/polymer grafting method that could be controlled and activated during the nanocomposite fabrication process. The approach consisted of a "grafting to" method: functionalization of the CNT with a molecule that can bond and anchor to the polymer chain, with the anchoring reaction activated by the use of UV irradiation. UV irradiation was chosen for its simplicity and ease of intensity, frequency, wavelength, and exposure time variation. In addition, the low consumption of energy and lack of volatile organic solvents made the use of UV technology very attractive, while the short wavelength of the UV light allows for precise focusing, providing the ability for selective exposure to areas of the composite [29]. Another benefit was that UV light can be used at ambient temperature and in the presence of air, thus avoiding any thermal degradation of the polymer [20]. An advantage of most photoreactive groups is the chemical inertness in the absence of light [21]. This assures that any interfacial interaction between the filler and matrix is solely a result of the applied external stimulus.

The photoreactive molecule of interest was benzophenone (BP), with the chemical structure as shown in Fig. 1.2. The light absorbance of BP has a wide range from 310 to 390 nm wavelength. BP can be effectively excited to a diradical triplet state using UV light in this wavelength range, to form a bond with an alkyl group after hydrogen abstraction (see Fig. 1.2) [21, 30, 31]. This behavior makes BP attractive since it can attach to various polymer backbones or side groups that contain a C-H bond.

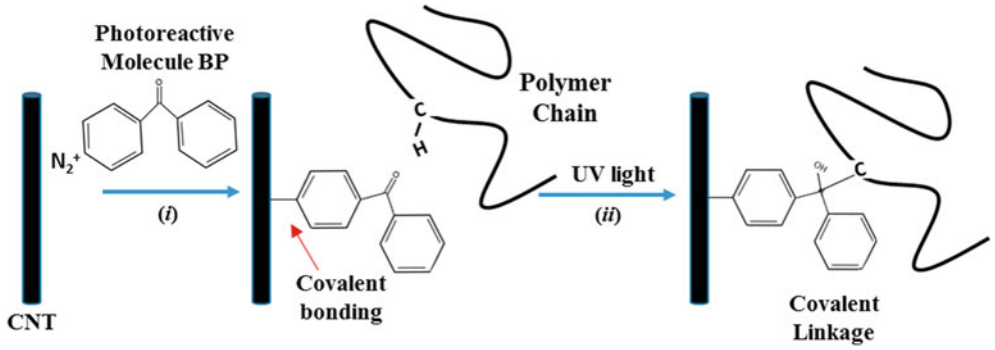

Fig. 1.2 Photoreactive benzophenone (BP) molecule bonded to a CNT via *(i)* diazonium reaction and subsequent *(ii)* photoreactive bonding to a polymer chain forming a covalent link between the CNT and polymer chain

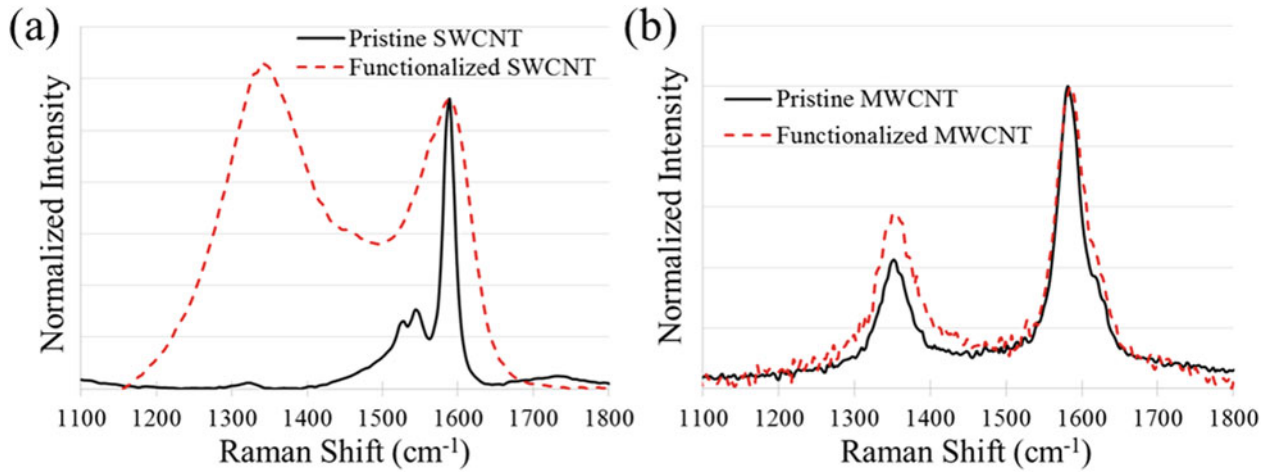

Fig. 1.3 Normalized Raman spectra of (**a**) pristine and functionalized HiPco SWCNTs and (**b**) pristine and functionalized MWCNTs

The approach was to chemically bond a BP molecule to a CNT such that when exposed to UV light, the BP would react and bond to the C-H bonds on the side groups or backbone of the polymer matrix, as schematically shown in Fig. 1.2. This photoreactive molecule would provide a controlled covalent link between the CNT and polymer chain.

The orientation of the filler is considered extremely important as the effect of this chemical bonding enhancement on the interfacial mechanics might not be observable if additional mechanisms are introduced as a result of misorientation. Studying the effect of CNT alignment provided a more theoretically grounded understanding of the interfacial load transfer mechanics.

1.3.1 Characterization of CNT Functionalization

In the Raman spectrum of a CNT, the peak ratio of the defect-derived D-band and the graphitic structure-derived G-band is a good indicator of the defect concentration in a CNT sample [27, 28, 32]. In Fig. 1.3a, the spectra of dispersed pristine HiPco SWCNTs is shown. It is observed that a high-intensity G peak (1600 cm^{-1}) and low-intensity D peak (1350 cm^{-1}) are present in the pristine sample, which indicates a low number of defect sites. After the reaction, a significantly enhanced D peak (at around 1350 cm^{-1}) is observed, resulting in a D/G peak ratio > 1, indicative of a high quantity of defects caused by grafting of the BP molecule to the CNTs. The same chemistry was effective for funtionalizing both SWCNT and MWCNT films. The Raman spectra (Fig. 1.3b) shows the enhanced D/G ratio after the reaction for aligned MWCNT films. It is worth mentioning that a D peak with considerable intensity was observed for the pristine MWCNT sample, which is due to the defects generated in the synthesis process [33]. Therefore, only a slight enhancement of D/G ratio can be observed for the functionalized sample, however the result does verify the attachment of the BP molecule to the surface of the aligned MWCNTs.

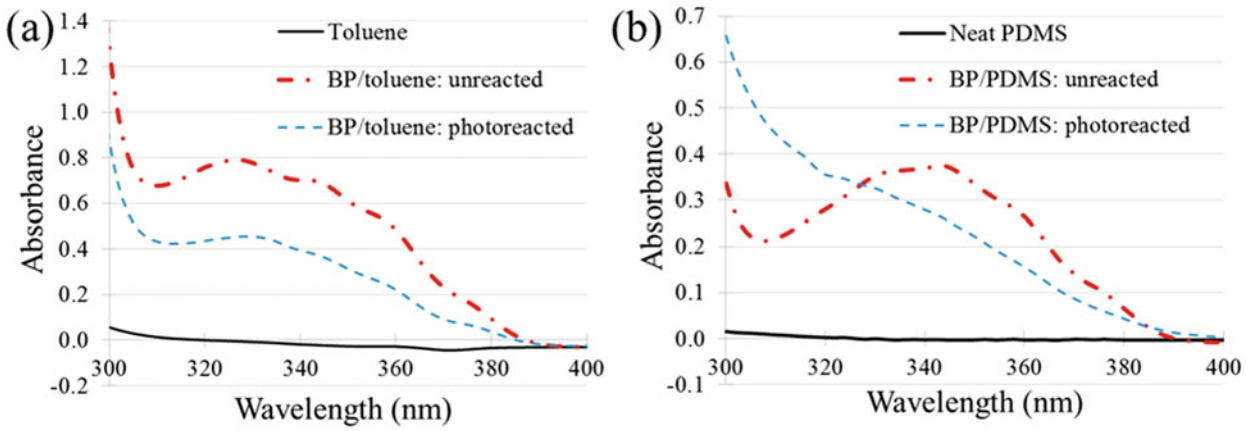

Fig. 1.4 Absorbance spectra of (**a**) BP dispersed in toluene before and after photoreaction and (**b**) BP embedded in PDMS before and after photoreaction. Results are for an irradiance of 500 mW/cm^2 and exposure time of 5 min

1.3.2 Photoreaction of Benzophenone

UV-vis spectroscopy was used to study the photoreaction of benzophenone both in a solvent and embedded in PDMS. As observed in Fig. 1.4a, the characteristic BP peak decreases with UV exposure. This result indicates that the irradiance and exposure time is sufficient to excite the BP molecule into a diradical triplet state and trigger a reaction with a C-H bond. The decrease of the characteristic peak indicates that less BP is available to absorb UV light and thus has reacted with the surrounding solvent molecules. Once embedded in PDMS, BP shows a significant decrease in the absorbance peak indicative of a reaction with the surrounding PDMS matrix.

1.3.3 Mechanical Behavior of CNT/PDMS Nanocomposites

The interfacial interaction, and thus the load transfer mechanisms, in CNT/polymer composite materials can result from a combination of the following: (1) mechanical interlocking, (2) van der Waals interactions, and (3) chemical bonding [34]. While mechanical interlocking results from surface topography on the CNT and the matrix conforming to that surface, van der Waals and chemical bonding are a function of the chemistry present at the interface. It is expected that an increase in interfacial interactions will lead to increases in elastic modulus and yield stress due to the increased efficiency of load transfer between the filler and matrix.

Evidence of improved interfacial interaction between the SWCNT film and the surrounding matrix is observed upon exposure to the UV stimulus. By triggering the photochemical covalent bonding, results in Fig. 1.5a show an increase of 22% in the elastic modulus after UV exposure compared to the functionalized case with no UV treatment.

Even though the SWCNT composites do show some slight nonlinearity, it is difficult to conclude at what point the composite yields by failure at the interface between the CNTs and matrix. This is a direct result of the random distribution of CNTs in the composite. If any interface failure occurs, it will happen over a wide range of stresses since the CNTs are not aligned in the direction of loading, thus the reason for the broad nonlinear response. Another effect of the random distribution is weak interparticle load transfer. As seen in Fig. 1.1a, there is substantial CNT-CNT interaction which could result in weak load transfer and thus would not significantly contribute to the composite modulus enhancement. Another possibility is the difficulty of PDMS penetration of the film. It is necessary for the polymer to penetrate the film in order for the polymer to act as the bridge between CNTs, as has been reported [1]. If so, only the outer CNT film surface would effectively bond with the surrounding matrix and thus the weak interparticle forces would dominate the interior of the film, resulting in weak stress transfer.

In order to address the issues observed in the SWCNT thin film results, a different approach to composite fabrication was taken which involved drawing of CNTs from a vertical forest. This procedure results in a less dense film as observed in Fig. 1.1b, allowing for the interpenetration of the PDMS chains. In addition, aligned CNTs would allow us to conclude that any observed reinforcement behavior is due solely to interfacial effects and not increased interactions between entangled CNTs since the reinforcements are in the direction of loading, similar to aligned discontinuous fiber composites. By aligning the

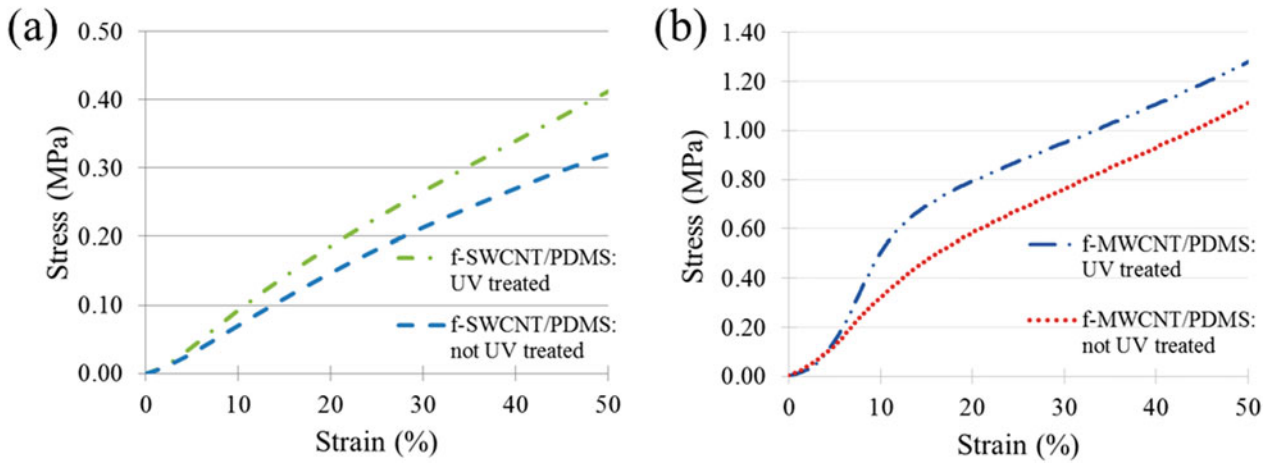

Fig. 1.5 Stress vs strain response for (**a**) randomly oriented functionalized SWCNT (f-SWCNT) film in a PDMS matrix and for (**b**) aligned functionalized MWCNT (f-MWCNT) film in a PDMS matrix, with and without exposure to a UV stimulus of 500 mW/cm^2 for 5 min

CNTs in the direction of loading, any observable change in the mechanical response would be due to altered interfacial interactions. The alignment will suppress any matrix yielding not associated with the interface and reduce CNT-CNT interaction phenomena.

The mechanical response of the aligned CNT composites is shown in Fig. 1.5b. At low strains (< 3%), all composite types show a similar elastic modulus. This behavior is as a result of the CNT films not being perfectly aligned to the loading direction but containing some initial waviness, as observed in Fig. 1.1b. As the composite material is further loaded, the waviness decreases and the CNTs further align in the direction of loading and thus show an onset in interfacial load transfer characterized by increased Young's modulus (at about 3% strain). The elastic modulus of the composite is measured past this onset point.

Results show a more pronounced yielding as compared to the SWCNT results, with a yield stress of 0.49 and 0.66 MPa for the non-UV treated and UV treated MWCNT composite samples, respectively. The UV-triggered enhanced interfacial interactions in MWCNT composites lead to a more defined and enhanced yield stress, with a total increase of 35%. In the non-UV treated samples, any interfacial interactions are due solely to mechanical interlocking and van der Waals. Upon exposure to UV light, the covalent bonding was triggered resulting in significant increase in elastic modulus from 3.88 to 7.50 MPa (93% increase) for a 5 min UV exposure time. In addition, the yielding of the composite became less broad and more defined. These results point to the significance of CNT-polymer interface engineering for enhancing and controlling the stiffness and yield stress of a composite.

In order to verify that the interface failed and that the observed enhancement was due solely to interfacial interaction, the composites were reloaded and the corresponding stress vs strain behavior captured. The enhancement in modulus due to the presence of the CNTs was lost (results not shown here) and the behavior followed that of the neat PDMS. The stress transfer at the interface deteriorated and thus the CNTs no longer carried any load, thus the reason for the response becoming similar to that of the neat matrix. This behavior was observed for every sample type. This verifies that the enhancement observed in the UV treated samples was due to enhanced interfacial interaction between the CNT and the surrounding matrix. Furthermore, this suggests a chemical bond interaction as would be expected by the covalent bond induced by the photoreactive molecule, as a broken covalent bond will not naturally re-form for another loading cycle.

In a random CNT case, it is difficult to convincingly conclude that modulus enhancement (and onset of interfacial failure) is solely due to increased interfacial interaction since many other effects (such as CNT entanglement, agglomeration, matrix tearing, curvature) are present, which affect the composite response. In addition, the stress distribution at the interface is not symmetric in off-aligned cases [35], which would result in a broad distribution of the onset of interfacial failure within the composite, making it difficult to pinpoint the onset of failure in the global mechanical response, thus the reason for the observed broadend behavior in the SWCNT composites. However, one can obtain a clearer, more theoretically grounded understanding of the interfacial load transfer mechanics by considering aligned CNT nanocomposites [8]. As our results show, interfacial effects are more pronounced in aligned composites, while in the unaligned CNT reinforcement, there are various mechanisms present that can result in not only less enhancement in mechanical properties, but also in a difficulty with isolating the salient mechanics.

1.4 Conclusion

The feasibility of using stimulus responsive chemistry to control the degree of interfacial interaction between a CNT filler and polymer matrix was studied. Both aligned and randomly oriented CNTs were functionalized with the photoreactive molecule benzophenone. Covalent bonding with the surrounding matrix was triggered by exposure to UV light at a 365 nm wavelength. Improved adhesion in randomly dispersed SWCNT composites was observed upon UV exposure, evident in the increase in elastic modulus of 22%. Aligned MWCNT film composites showed a more significant increase in elastic modulus and yield stress. The alignment of the CNTs not only allowed for the CNTs to sustain load, but also suppressed any matrix yielding not related to interfacial stresses and minimized any CNT-CNT interaction, thus resulting in an enhancement in elastic modulus of 93% when comparing UV treated and non-treated CNT composites. Repeated loading of the samples verified that the reinforcement behavior was due to solely interfacial interactions as the composites behaved like the neat PDMS material. This work shows the potential of using stimulus-responsive interfacial adhesion as a means to controlling interfacial mechanics in CNT/polymer nanocomposites.

Acknowledgement F. Gardea and Z. Huang contributed equally to this work. This work is partially supported by the Army Research Office under Cooperative Agreement No. W911NF1420024 and the Air Force Office of Scientific Research through Grant No. FA9550-16-1-0150.

References

1. Coleman, J.N., et al.: Small but strong: A review of the mechanical properties of carbon nanotube–polymer composites. Carbon. **44**(9), 1624–1652 (2006)
2. Gardea, F., Lagoudas, D.C.: Characterization of electrical and thermal properties of carbon nanotube/epoxy composites. Compos. Part B. **56**, 611–620 (2014)
3. Biercuk, M., et al.: Carbon nanotube composites for thermal management. Appl. Phys. Lett. **80**(15), 2767–2769 (2002)
4. Rittigstein, P., et al.: Model polymer nanocomposites provide an understanding of confinement effects in real nanocomposites. Nat. Mater. **6**(4), 278–282 (2007)
5. Schadler, L.: Nanocomposites: Model interfaces. Nat. Mater. **6**(4), 257–258 (2007)
6. Schadler, L., Brinson, L., Sawyer, W.: Polymer nanocomposites: A small part of the story. JOM. **59**(3), 53–60 (2007)
7. Schadler, L.S., et al.: Designed interfaces in polymer nanocomposites: A fundamental viewpoint. MRS Bull. **32**(04), 335–340 (2007)
8. Gardea, F., et al.: Energy dissipation due to interfacial slip in nanocomposites reinforced with aligned carbon nanotubes. ACS Appl. Mater. Interfaces. **7**(18), 9725–9735 (2015)
9. Koratkar, N.A., et al.: Characterizing energy dissipation in single-walled carbon nanotube polycarbonate composites. Appl. Phys. Lett. **87**(6), 063102 (2005)
10. Suhr, J., Koratkar, N.A.: Energy dissipation in carbon nanotube composites: A review. J. Mater. Sci. **43**(13), 4370–4382 (2008)
11. Wang, S., Qiu, J.: Enhancing thermal conductivity of glass fiber/polymer composites through carbon nanotubes incorporation. Compos. Part B. **41**(7), 533–536 (2010)
12. Hong, W.-T., Tai, N.-H.: Investigations on the thermal conductivity of composites reinforced with carbon nanotubes. Diamond Relat. Mater. **17**(7), 1577–1581 (2008)
13. Park, J.J., et al.: Functionalization of multi-walled carbon nanotubes by free radical graft polymerization initiated from photoinduced surface groups. Carbon. **48**(10), 2899–2905 (2010)
14. Liu, P.: Modifications of carbon nanotubes with polymers. Eur. Polym. J. **41**(11), 2693–2703 (2005)
15. Qin, S., et al.: Functionalization of single-walled carbon nanotubes with polystyrene via grafting to and grafting from methods. Macromolecules. **37**(3), 752–757 (2004)
16. Ma, P.-C., et al.: Dispersion and functionalization of carbon nanotubes for polymer-based nanocomposites: A review. Compos. A: Appl. Sci. Manuf. **41**(10), 1345–1367 (2010)
17. Ramanathan, T., et al.: Functionalized graphene sheets for polymer nanocomposites. Nat. Nanotechnol. **3**(6), 327–331 (2008)
18. Sahoo, N.G., et al.: Polymer nanocomposites based on functionalized carbon nanotubes. Prog. Polym. Sci. **35**(7), 837–867 (2010)
19. Zhao, Y.: Functionalization of single-walled carbon nanotubes (SWNTs) with stimuli-responsive dispersants. Mod Chem Appl. **1**(3), 1–2 (2013)
20. Decker, C., et al.: Synthesis of nanocomposite polymers by UV-radiation curing. Polymer. **46**(17), 6640–6648 (2005)
21. Prucker, O., et al.: Photochemical attachment of polymer films to solid surfaces via monolayers of benzophenone derivatives. J. Am. Chem. Soc. **121**(38), 8766–8770 (1999)
22. Huang, J., et al.: Covalently functionalized double-walled carbon nanotubes combine high sensitivity and selectivity in the electrical detection of small molecules. J. Am. Chem. Soc. **135**(6), 2306–2312 (2013)
23. Ng, A.L., et al.: Chemical gating of a synthetic tube-in-a-tube semiconductor. J. Am. Chem. Soc. **139**(8), 3045–3051 (2017)
24. Li, Y.L., Kinloch, I.A., Windle, A.H.: Direct spinning of carbon nanotube fibers from chemical vapor deposition synthesis. Science. **304**(5668), 276–278 (2004)
25. Huynh, C.P., Hawkins, S.C.: Understanding the synthesis of directly spinnable carbon nanotube forests. Carbon. **48**(4), 1105–1115 (2010)
26. Nikolaev, P., et al.: Gas-phase catalytic growth of single-walled carbon nanotubes from carbon monoxide. Chem. Phys. Lett. **313**(1), 91–97 (1999)

27. Kim, M., et al.: Fluorescent carbon nanotube defects manifest substantial vibrational reorganization. J. Phys. Chem. C. **120**(20), 11268–11276 (2016)
28. Piao, Y.M., et al.: Brightening of carbon nanotube photoluminescence through the incorporation of sp(3) defects. Nat. Chem. **5**(10), 840–845 (2013)
29. Srinivasan, R.: Ablation of polymers and biological tissue by ultraviolet lasers. Science. **234**(4776), 559–565 (1986)
30. Dorman, G., et al.: The life of Pi star: Exploring the exciting and forbidden worlds of the benzophenone photophore. Chem. Rev. **116**(24), 15284–15398 (2016)
31. Dorman, G., Prestwich, G.D.: Benzophenone photophores in biochemistry. Biochemistry. **33**(19), 5661–5673 (1994)
32. Deng, S., et al.: Confined propagation of covalent chemical reactions on single-walled carbon nanotubes. Nat. Commun. **2**, 382 (2011)
33. Qian, W.Z., et al.: The evaluation of the gross defects of carbon nanotubes in a continuous CVD process. Carbon. **41**(13), 2613–2617 (2003)
34. Schadler, L., Giannaris, S., Ajayan, P.: Load transfer in carbon nanotube epoxy composites. Appl. Phys. Lett. **73**(26), 3842–3844 (1998)
35. Kopp, R., et al.: Multi-fidelity modeling of interfacial micromechanics for off-aligned polymer/carbon nanotube nanocomposites. In: 58th AIAA/ASCE/AHS/ASC Structures, Structural Dynamics, and Materials Conference, 2017

Chapter 2
Devulcanized Rubber Based Composite Design Reinforced with Nano Silica, Graphene Nano Platelets (GnPs) and Epoxy for "Aircraft Wing Spar" to Withstand Bending Moment

A. B. Irez, E. Bayraktar, and I. Miskioglu

Abstract This paper aims a new composites design by using devulcanized recycled rubber (90 wt %) and epoxy 20 wt %) based composites reinforcement with nano silica and graphene nano plates (GnPs). The toughening effects of nano-silica/graphene hybrid filler at various ratios on this composite were investigated for aircraft engineering applications especially aircraft wing spar. As well known, wing spar is used two of them; one front, other rear in order to control torsional effect of the wing. Nano-silica and graphene nano plates (GnPs) have been used as the main reinforcing fillers that increase the usefulness of recycled rubber composite. As each filler retains its specific advantages, the use of nano-silica/graphene combinations should improve the mechanical and dynamic properties of recycled rubber composite.

In aircraft and aerospace applications, graphene nano plates can be used effectively new design of electrically conductive composites which can improve the electrical conductivity of these composites designed for the fuselages that it would replace copper wire which is generally used for the prevention of damage caused from lightning strikes. There are many advantages and possibilities that graphene nano plates (GnPs) can prevent water entering the wings, which adds weight to the aircraft.

In the frame of this present common research, a new devulcanized recycled rubber based composite design for aircraft wing spar has been proposed and wing load due to structure weight was calculated analytically to tolerate bending moment under the service conditions. The toughness properties and tribological behaviour indicating the reinforcement of recycled rubber based composite were evaluated. Microstructural and fractural analyses were made by Scanning Electron Microscopy (SEM).

Keywords Recycled Composites · Devulcanized Rubber · Reinforcement effect · Static 3P-Bending · Bending Moment · Analytical Model

2.1 Introduction

Rubber generally provide a good heat resistance, ease of deformation at ambient temperatures and exceptional elongation and flexibility before breaking. These properties have established rubber as excellent and relatively cheap materials for various applications in many manufacturing areas [1–9]. However, utilization of the recycled rubber for the manufacturing of the new composites is a very economical way for cost effective composite design. Last decades, the usage of the recycled rubber obtained from fresh and clean scrap rubber for different industrial applications such as automotive and aeronautical engineering has been very well developed as very useful material for the composites either as a matrix or as a reinforcement. Extensively, this rubber powder come directly manufacturing of sportive affaires, shoes etc., For this reason, it is feasible to use it after chemical (silanization) and devulcanization treatments for cost effective composite design [3, 5, 8, 9].

Reinforcement of the rubber based composites with nano graphene and/or graphene nano plates (GnPs) are very extensive applications in composite design for mainly aeronautic and aerospace applications. Graphene are known and used widely used as multi- functional reinforcement materials that can improve the electrical, piezo-resistive, dielectric, thermal, and

A. B. Irez
CentraleSupélec, Université Paris-Saclay, Gif-sur-Yvette, France

E. Bayraktar (✉)
Supmeca-Paris, School of Mechanical and Manufacturing Engineering, Saint-Ouen, Paris, France
e-mail: bayraktar@supmeca.fr

I. Miskioglu
Michigan Technology University, Engineering Mechanics Department, Houghton, MI, USA

P. R. Thakre et al. (eds.), *Mechanics of Composite, Hybrid and Multifunctional Materials, Volume 5*, Conference Proceedings of the Society for Experimental Mechanics Series, https://doi.org/10.1007/978-3-319-95510-0_2

mechanical properties of rubber based composites even at extremely lower loadings. Because of the exceptionally high surface area, as compared to other graphite derivatives, an enormous improvement in properties is observed for graphene composites. Correspondingly, they exhibit unique advantages, as compared with all other organic and inorganic fillers, and are thus useful in many applications. The interactions between the various elements of a complex multicomponent system, such as the ones found in graphene/rubber nanocomposites, play a major role on the final physico-chemical properties of the material. For this reason, in much of the literature, surface chemistry is applied to the different components of the system, in order to ensure chemical compatibility between them. In addition, it can lead to the formation of chemical bonds focused towards the improvement of the properties of the initial material and a satisfactory dispersion of the filler due to very high Young's modulus (1 TPa) and intrinsic strength of single graphene sheet 130 GPa [1].

As for the reinforcement of the rubber based composites with nano silica (SiO_2 d < 15–30 nm) particles [10–12] can also increase toughening of the rubber based composites and its distribution in matrix is very easily managed that give a multiphase hybrid-toughened composite structure. The rubber based composites reinforced with nano silica and graphene nano plates (GnPs) show higher thermal conductivity of rubber based composites containing of nano silica and GnPs in a certain ratio.

In the frame of this present common research, a new devulcanized recycled rubber based composite design for aircraft wing spar has been proposed and wing load due to structure weight was calculated analytically to tolerate bending moment under the service conditions. The toughness properties and tribological behaviour indicating the reinforcement of recycled rubber based composite were evaluated. Microstructural and fractural analyses were made by Scanning Electron Microscopy (SEM). We believe that this new composite design by using nano silica and graphene nano plates may exposed a novel interface design approach for developing multifunctional rubber based composites in order to manufacture of aircraft wing spar in safety conditions.

2.2 Experimental Conditions

2.2.1 Materials Processing

The use of recycled rubbers within epoxy matrix is a subject of interest requiring particular processes of the rubber particles. Due to the previously conducted vulcanization process, cross-linked structure of rubber restrains the movement of rubber chains and limit the interaction forces between scrap rubber particles and epoxy matrix. In consequence, a reduction in the performance of final product is observed [1–3]. In this case, to enhance materials properties of the final product, devulcanization operation is recommended. In the frame of the current work, the energy for devulcanization was provided by microwaves and it is followed by chemical surface treatments. In this study, at the beginning of the process, recycled rubber particles were blended with solid bisphenol-A type epoxy powders in pre-defined mass rates.

However, because of the insufficient free chains of rubber particles, formation of a robust and durable bonding between epoxy and recycled rubber is quite challenging. For this reason, fresh scrap rubber should be devulcanized. In fact, devulcanization is known to be an operative practice for manufacture of recycled rubbers to increase flowing capacity and also to be remoulded during manufacturing of new designed composites.

During this process, formerly created sulphur links are tried to be broken and also new other links are generated, it means that the structure of the material is modified entirely as renewable process. Thanks to this process, newly created free chains make possible have chemical bonding between rubber and epoxy [1–5, 13, 14].

A new design of devulcanized rubber based composite, reinforced with nano silica and graphene nano platelets (GnPs) are prepared in several steps:

1. Chemical treatment was applied on rubber. The principal of the chemical treatment consists in a short silanization process followed by acrylic acid followed by silanization in order to activate the surface of the rubber particles.
2. After drying of the chemically treated rubber powders, they are exposed to short microwave heating in two stages during 4 min under 900 W of power in order to avoid degradation of the main chains called devulcanization.
3. At the final stage, devulcanized rubber were mixed with a little amount of epoxy resin powders for binding of rubber matrix and reinforcements. This mixture used as a matrix after that the new designed composites are manufactured by using classical powder metallurgy methods.
4. After the mixture of the reinforcements (here nano silica and GnPs) in the matrix, a fast-rotating toothed-wheel milling process was carried out during 4 h to obtain fine rubber powder.

Table 2.1 Composition of the epoxy-rubber based composites

Devulcanized rubber based composite Rubber – Epoxy (%20 Epoxy – 80 Rubber)	CJ I	CJ II	CJ III
Reinforcements (wt %)	10 $SiO_2$4 GnPs	10 $SiO_2$6 GnPs	10 $SiO_2$8 GnPs

Table 2.2 Hardness values of CJ specimens

Hardness measurement	
Specimen	Shore D
CJ I	80.8
CJ II	77.4
CJ III	76.6

Table 2.3 Density values of CJ specimens

Hardness measurement	
Specimen	Density (g/cm^3)
CJ I	1.47
CJ II	1.45
CJ III	1.44

5. After having a homogeneous powder compound, the composite specimens were manufactured by using double uniaxial action press at a temperature of 180 °C under a pressure of 70 MPa during the heating of 30 min.
6. All of the specimens (30/50 mm in diameter) were cooled slowly in the press. All of the specimens were post-cured isothermally at 80 °C for 24 h.

This combined method consists exposing recycled rubbers to microwave heating in a short time pursued by a pre-chemical treatment that is applied in practical point of view. Thus, a good cohesion is provided at the interface between epoxy resin and devulcanized rubber powders to improve the properties of the recycled rubber with a particle size varying from 10 to 100 μm. obtained from fresh-clean scrap rubbers coming from the production of the sportive equipment. It means that they are fresh, clean and completely different from ground tire. The compositions of the nano silica and GnPs reinforced recycled rubber based composites (called as CJ I-II-III hereafter) were given in Table 2.1.

As seen the reinforcement percentages in the rubber matrix, the combination of SiO_2/GnPs for each composition gives a good adhesion of nano silica and GnPs to the rubber 80 wt% + Epoxy 20 wt%.

2.2.2 Mechanical, Microstructure, Fracture Surface Analyses and Shore-D Hardness Measurements

Fracture surface damage analyses and microstructural observation have been realized by means of optical (OM) and scanning electron microscopy (SEM). SEM observation was realized on fracture surface of the tested specimens with Scope/JSM-6010LA Jeol® electron microscope.

Surface hardness measurements of the specimens were performed after post curing. Shore D hardness test measurements on the polished flat surfaces of the specimens were carried out according to ASTM D 2240 using Shore D hardness tester, (type HBD-100-0). Hardness results were given in Table 2.2.

Three-point bending tests (3 PB) have been carried out according to the ASTM D790 standards. Tests were realized with the machine Zwick Proline Z050TN and during the tests crosshead speed was selected as 1 mm/min. Flexural strength and strain were obtained from the test results. At least three specimens for each composition were used and standard deviation and average values were given in results chapter with standard deviation values. In addition, fractural properties such as plain strain fracture toughness (K_{Ic}) and critical strain energy release rate (G_{Ic}) were investigated with SENB specimens and the tests were realized according to ASTM D5045 standard. Notches were introduced by tapping a fresh razor blade. Impact response of the three composites were compared with an in-house designed drop weight impact test machine. A 1.9 kg conical punch was used for the tests, punch height was 900 mm and with an impact velocity of 4 m/s.

After preparation of the specimens, densities of the compositions were measured and they were given in Table 2.3.

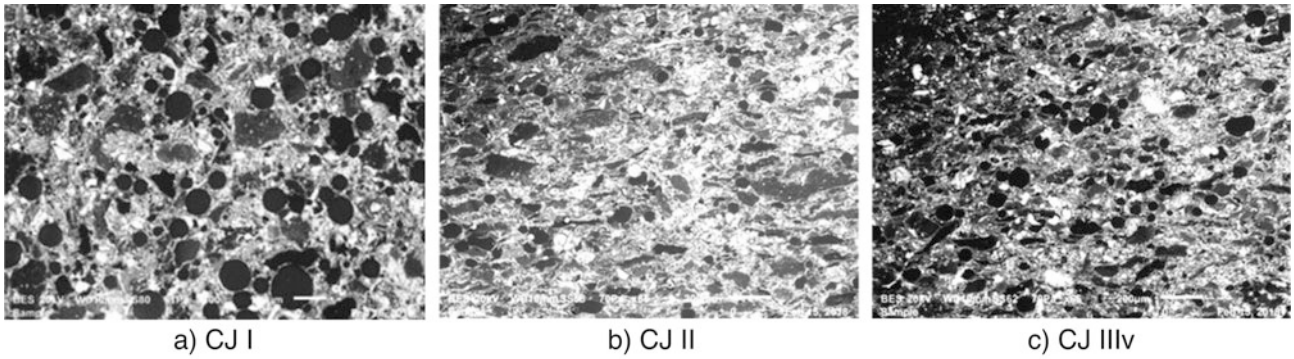

Fig. 2.1 Microstructure of the composites developed for the wings spars for this research (**a**) CJ I (**b**) CJ II (**c**) CJ III

2.2.3 Wear Resistance (Scratch Test) and Damage Analysis Via 3D Optical Roughness Meter

In the current research basic idea on the tribological behaviour of the epoxy and recycled elastomer based composites was evaluated performing scratch tests. A 3D optical surface scanner was utilized to assess damage zone after the scratch test in terms of scratch depth and average scratch roughness. Scratch were created over the polished specimens in two different loading conditions (10–15 N) for ten cycles on the same amplitude by using Anton Paar™ MST^3 micro scratch tester.

2.3 Results and Discussions

2.3.1 Microstructural Evaluation of the Composites

After hot compaction, sectioning was made then mounted specimens were polished. Then, general microstructures of the each composites were observed and they were shown in Fig. 2.1.

Then, mapping analyses was carried out for each composition were presented in Fig. 2.2 with together the general microstructures of the each composition. This type of analyze allows us to observe the distribution of the reinforcements in the matrix. It seems that a homogenous distribution of the reinforcements in the structure for each composition.

2.3.2 Three Point Bending Tests and Fracture Surface Observation

Three-Point Bending (3 PB) tests have been carried out for each different type of compositions with at least three specimens.

Flexural stress is calculated during three-point bending test according to the Eq. 2.1:

$$\sigma = \frac{3Pl}{2bh^2} \tag{2.1}$$

In this formula, l is the span length, P is the maximal bending load, b and h are the sample thickness and depth, respectively.

Flexural strain, $\boldsymbol{\varepsilon_f}$, was determined according to the Eq. 2.2:

$$\varepsilon_f = \frac{6Dh}{l^2} \tag{2.2}$$

D is the maximum deflection at the center of the specimen.E_B is the modulus of elasticity in bending and it is expressed with the Eq. 2.3 as follows:

$$E_B = \frac{l^3 m}{4bh^3} \tag{2.3}$$

m is the tangent of the initial straight portion of the force-displacement curve.

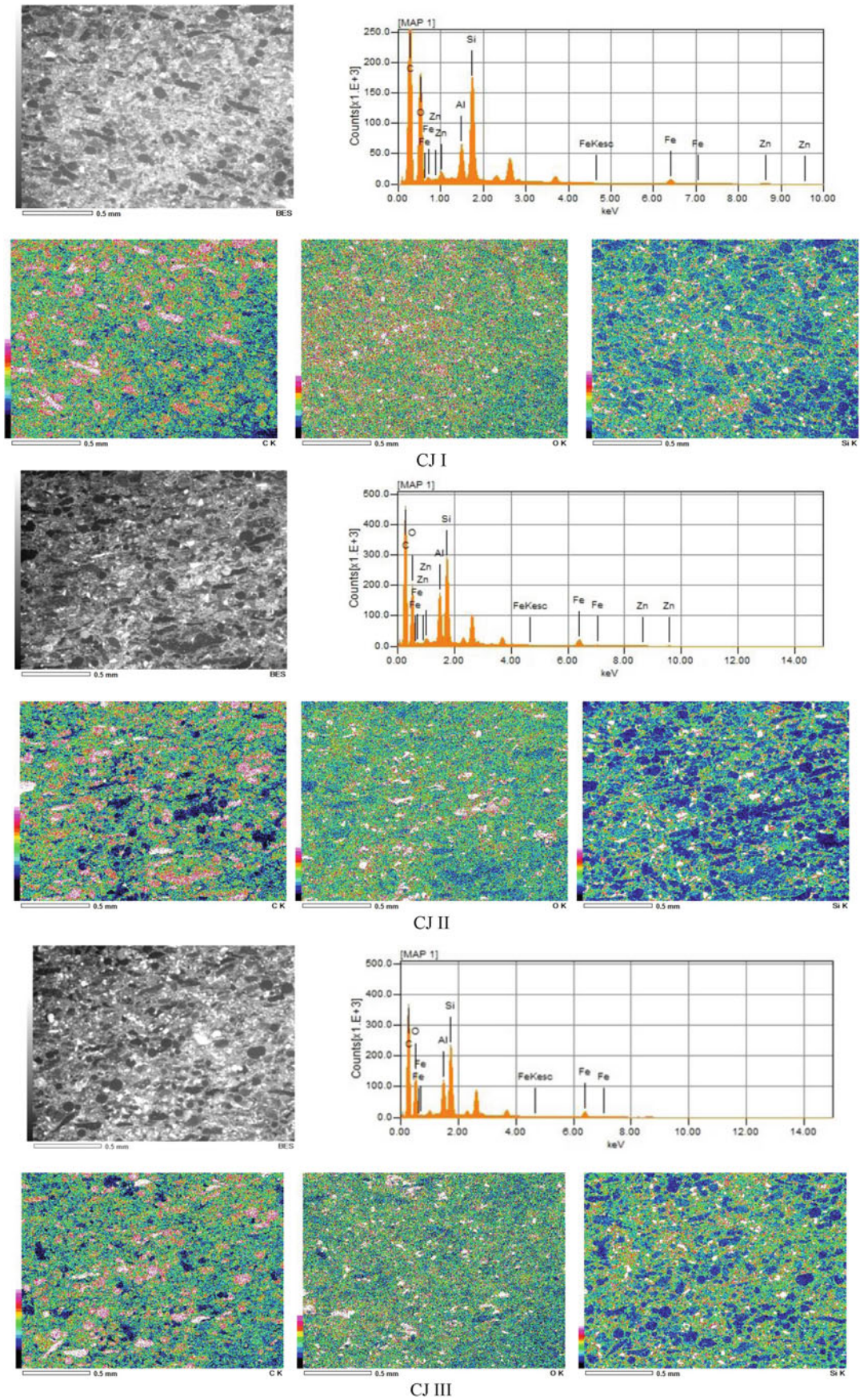

Fig. 2.2 Microstructure analysis with EDS together with Mapping for the composites CJ I CJ II and CJ III respectively

Table 2.4 Comparison of mechanical properties of CJ specimens

	Flexural stress (MPa)	Flexural modulus (MPa)	Strain in break (ε %)	K_{Ic} (MPa $m^{1/2}$)	G_{Ic} (kJ/m^2)
CJ I	15.76 ± 0.91	2.61 ± 0.28	0.348 ± 0.001	1.107 ± 0.027	0.649 ± 0.032
CJ II	11.23 ± 3.88	2.05 ± 0.93	0.359 ± 0.001	0.618 ± 0.091	0.138 ± 0.039
CJ III	15.03 ± 0.38	2.47 ± 0.066	0.363 ± 0.001	0.953 ± 0.065	0.367 ± 0.017

Table 2.5 Comparison of the experimental and analytic modelling results

Composition name	Experimental elasticity modulus	Elasticity modulus (Halpin – Tsai)	Relative difference
CJ I	2.61 ± 0.28	1.874	28%
CJ II	2.05 ± 0.93	1.937	5%
CJ III	2.47 ± 0.066	2.004	18%

The mode I fracture toughness, K_{Ic}, was determined by testing of the SENB specimens and K_{Ic} was calculated according to the Eq. 2.2:

$$K_{Ic} = \frac{F}{B\ w^{\frac{1}{2}}} f(x); \quad x = \frac{a}{W} \quad , 0 < \frac{a}{W} < 1 \tag{2.4}$$

F is the maximum force from the load-elongation plot; *B* is the thickness of the specimen; *W* is the width and "a" is the total notch length.*f(x)* is the geometry correction factor and is expressed with the Eq. 2.3 as follows:

$$f(x) = 6(x)^{0.5} \left\{ \frac{\left[1.99 - x\,(1-x)\left(2.15 - 3.93x + 2.7x^2\right]\right.}{(1+2x)\,(1-x)^{1.5}} \right\} \tag{2.5}$$

Critical strain energy release rate (fracture energy) G_{Ic} was calculated using the expression Eq. 2.4:

$$G_{Ic} = \frac{{K_{Ic}}^2\left(1-\upsilon^2\right)}{E} \tag{2.6}$$

where *E* is the elasticity modulus for plane stress approach examined for thin specimens.

Table 2.4 indicates the mechanical properties in bending mode. Fracture toughness values were also presented in the table.

Table 2.4 indicates that The hybrid rubber based composites reinforced with nano silica and graphene nano plates (GnPs) with a certain ratio have shown enhancements in the mechanical properties, and more significantly, fracture toughness (K_{IC}), which can be explained by synergistic impact coming from the intrinsic physical leftacteristics of the reinforcements it means that nano silica and graphene nano plates (GnPs). In this study, the highest K_{IC} can be obtained with addition of small amounts of graphene nano plates (GnPs). However, maximum strain values in break are the same levels.

After that, more detail analyses were given for the analytical modelling applied to three composites to compare their elasticity modulus by using experimental results. For these analyses, Halpin-Tsai model was chosen for the sake of its simplicity. Because this model is quite practical and it gives the well coherent results with the experimental methods in the case of homogeneous distribution of the fillers.

Halpin – Tsai's model was given in Eq. 2.7, where E_c, Ef and E_m are Young's modulus of the composite. V_f and V_m is the volume fraction of the AFs and the matrix, respectively. ξ is the shape factor of the fibers which is determined from the proportion of L, average length of the fibers and D, average diameter of the fibers.

$$\frac{E_c}{E_m} = \frac{1 + \xi\eta V_f}{1 - \xi\eta V_f}, \qquad \eta = \frac{\frac{E_f}{E_m} - 1}{\frac{E_f}{E_m} + \xi}, \qquad \xi = 2\,(\mathrm{L/D}) \tag{2.7}$$

According to the comparison this model with the experimental results, certain deviations are observed for the composites considered in this research. All of the results for three composites were presented in Table 2.5.

Fracture surfaces obtained from 3 PB tests have been analyzed by means of Scanning Electron Microscopy (SEM). It noticed that good adhesion of the both of the reinforcements in the rubber based matrix by creating an ideal interface for

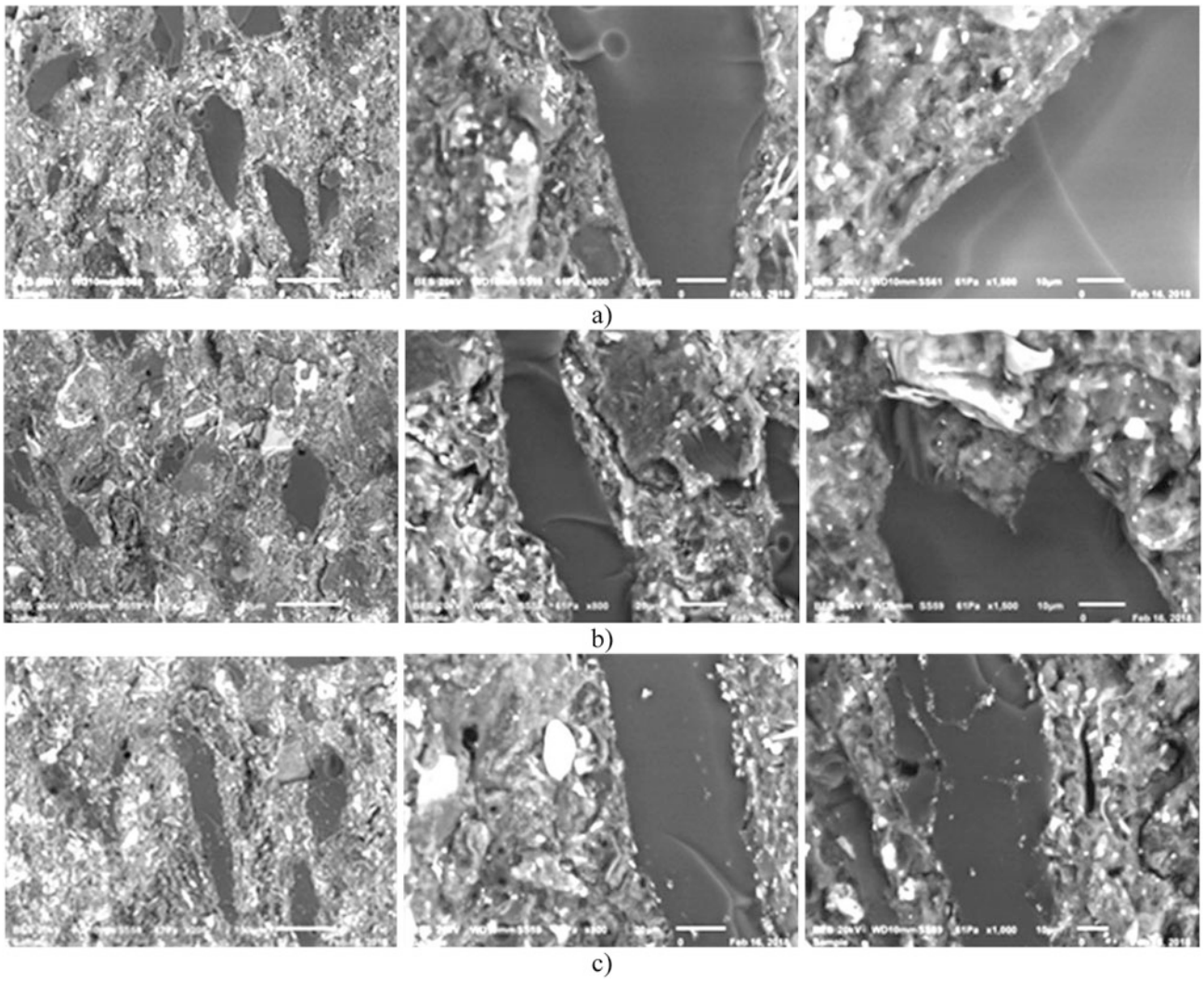

Fig. 2.3 (**a**) Fracture surfaces of the 3 different composites tested with 3P-Bending CJ I (**b**) CJ II (**c**) CJ III

each composition, as presented in Fig. 2.3 with different fracture surfaces taken by SEM. Cavitation and void formation in the rubber matrix with matrix expansion and locally, debonding of nano particles with consequent void growth have been observed in the structure as the improved toughening mechanisms. It seems also an interaction between devulcanized rubber and the epoxy is very fine and there is fusion mutually between them.

For this evolution, the mixture of devulcanized rubber (80 wt %) with epoxy (20 wt %) plays an important role. Some of the specimens with homogenous distribution of the nanoparticles have shown a typical debonding of the silica nanoparticles with GnPs that should be origins of the weakening of the matrix–particle interface. The toughness improvement in hybrid rubber based composites should be direct related to the increment of the debonding phenomena that can increase the size of the plastic zone in the structure. This case facilitate the devulcanized rubber based composites to dissipate additional fracture energy.

2.3.3 Drop Weight Testing

Drop weight test analyses have been carried out on the three composites for the measurement of the impact resistance and energy absorbance ability of the manufactured composites for wing spar. Four specimens were tested for each composite. Absorbed energies measured with maximum force during impact were presented in Table 2.6.

Table 2.6 Drop weight tests results on CJ specimens

Composition name	Maximum force (N)	Absorbed energy (J)
CJ I	2232.25 ± 34.68	1.27 ± 0.04
CJ II	2647.45 ± 29.94	1.49 ± 0.17
CJ III	3188.8 ± 348.74	1.66 ± 0.21

Table 2.7 Scratch test results for CJ compositions

Composition name	10 N		15 N	
	Worn surface (mm^2)	Worn volume (mm^3)	Worn surface (mm^2)	Worn volume (mm^3)
CJ I	1.32	0.0886	1.59	0.135
CJ II	1.16	0.0697	1.33	0.0972
CJ III	1.23	0.0811	1.73	0.136

From Table 2.6 it is clearly seen that GnPs improve the impact resistance of the composites. The maximum force during the impact is proportional to the absorbed energy [6, 7].Layered structure of GnPs is possibly enables to improve the damping characteristics of the composites.

Shortly, it is noticed that the absorbed energy for each specimen during the impact tests is related to the increment of the plastic zone in the structure due to the debonding of the nano particles. Higher dispersion of the values is also related to the test specimens prepared under laboratory conditions; hot compaction, cutting notch effect, etc.

2.3.4 Damage Analysis by Means of Micro Scratch Test and 3D Optical Surface Roughness Meter

After completing mechanical tests, tribological characterization of the composites were done by micro scratch tests. Three dimensional damages were observed three dimensionally by an optical surface scanner. The 3D damage results are presented in the Fig. 2.4.

Quantitative results related to scratch tests were given in Table 2.7. It seems that the increase of the reinforcement content, cause in the composites high resistance to wearing. In reality, because of the high shear stress at the interfaces the interfacial shear stress should probably be the main reason for damage of the matrix and reinforced filler interfaces. When the indenter is slipping, tangential tensile stress is caused on the surface behind the indenter, while in front of the indenter the tangential stress is compressive.

As expected higher force values resulted in higher damage traces. Damaged volume is significantly proportional with the force level. However, increasing force level did not manifest in the same manner for the damaged surface. In addition, increasing GnPs content generally improves the wear resistance for the composites in consideration.

2.3.5 Numerical Approach for These Composites

After realizing experimental procedures, mechanical test results were compared with finite element modelling (FEM). In FEM procedure, simplified approaches were utilized. In this regard, after generating 3D solid model of the tested specimens in 3 PB tests, these models were meshed with quadratic tetrahedral elements (C3D10).

After that, boundary conditions were applied according to two selected approach. In the first approach, maximum load obtained from the 3 PB tests was imposed to the material and maximum stress and the displacement in the critical region (z-direction) were obtained.

In the second approach, maximum deflection in the middle of the specimen which was obtained from 3 PB tests was imposed to the material and maximum stress in the middle of the specimen was determined. FE models were solved in linear elastic mode by using Abaqus FEM software.

First approach was executed and results were illustrated in Fig. 2.5.

The comparison of experimental and FEM results according to first approach was given in Table 2.8.

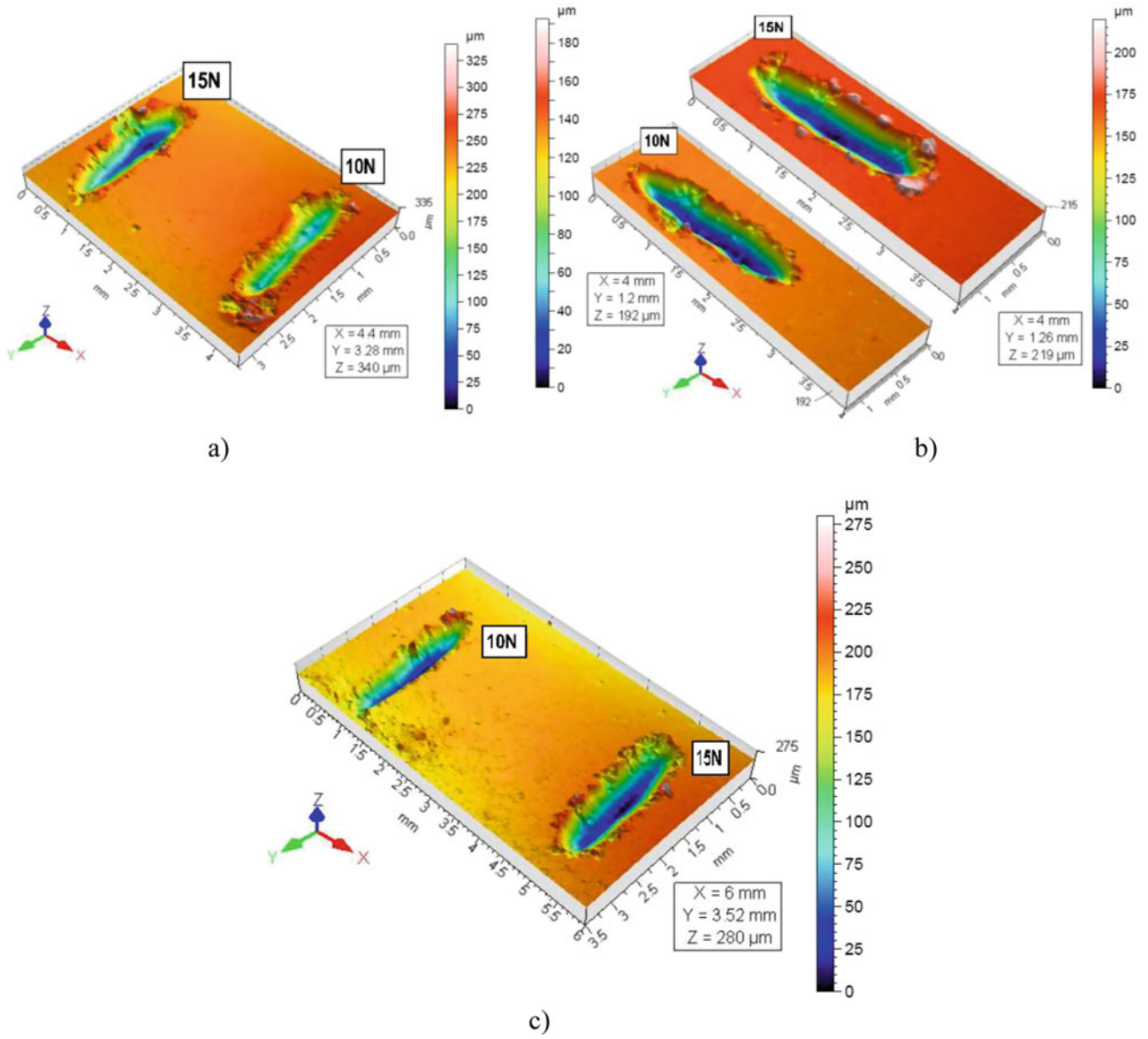

Fig. 2.4 Micro scratch test results carried out on the three compositions (**a**) CJ I (**b**) CJ II (**c**) CJ III, respectively

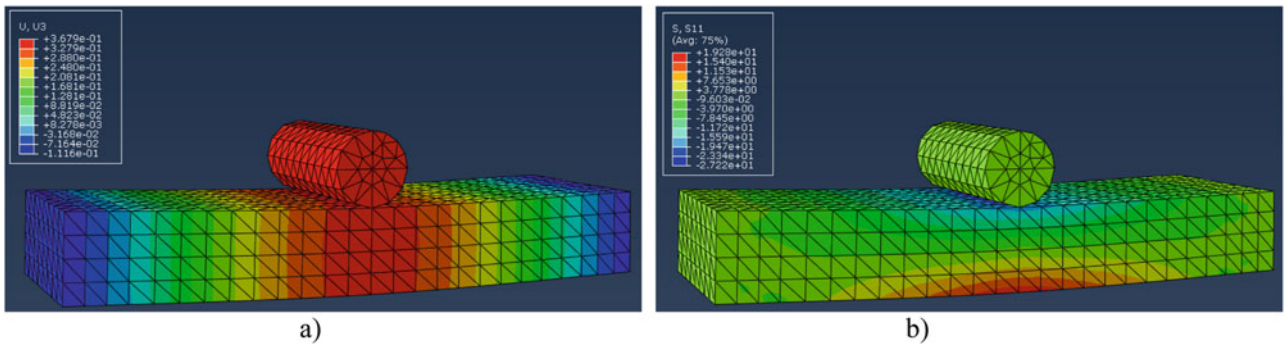

Fig. 2.5 FEM results according to maximum force approach (**a**) Displacement contour (**b**) Stress contour

According to Table 2.8, FEM gives coherent results for the stress values even if minor errors were observed. On the other hand, for the displacement, FEM does not give quite consistent results. After conducting second approach, all of the results are illustrated together in Fig. 2.6.

Table 2.8 Comparison of the modelling and experimental approaches for the imposed experimental F_{max}

1st approach: Applied load = Experimental F_{max}				
Composition name	Stress FEM (σ_{11} MPa)	Relative difference with experiments	Displacement max FEM (u_3 mm)	Relative difference with experiments
CJ I	19.28	25%	0.368	53%
CJ II	11.11	20.9%	0.214	25%
CJ III	17.33	17.33%	0.313	38%

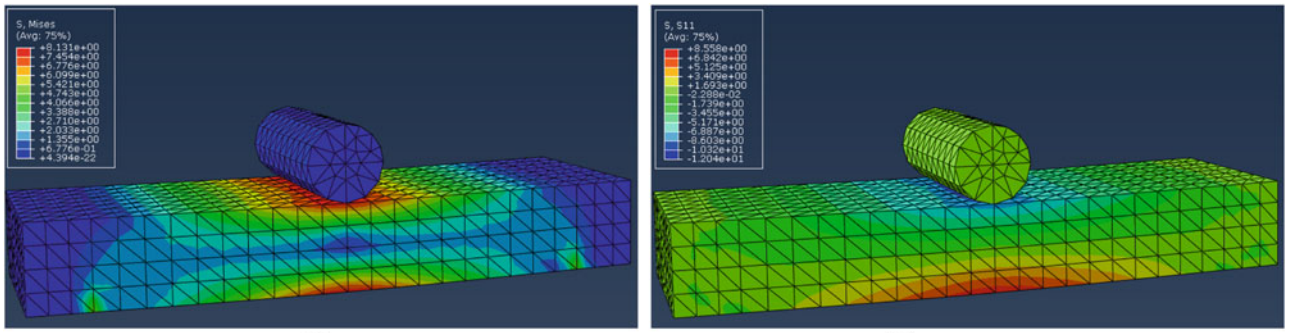

Fig. 2.6 FEM results according to maximum displacement approach (**a**) General Stress contour (**b**) σ_{11}

Table 2.9 Comparison of the modelling and experimental approaches for the imposed experimental D_{max}

2nd approach: Applied displacement = Experimental D_{max}	
Stress FEM (σ_{11} MPa)	Relative difference with experiments
8.42	46%
12.55	27%
8.85	32%

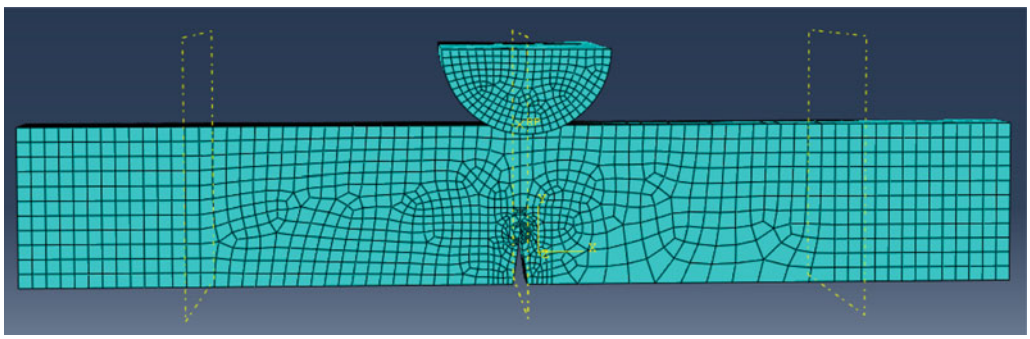

Fig. 2.7 Meshed model for SENB specimens

In this figure, the critical region was shown as the middle of the specimen as expected. Also, from these figures, the stress in the top of the sample is compressive whereas in the bottom tensile (Table 2.9).

By comparison of these two approaches, it is noticed that first approach gives more coherent results to estimate stress values. On the other hand, estimation of the displacement values requires more detailed modelling considerations.

After modelling of 3 PB results, another simplified model to estimate fracture toughness was applied to these composites. This time, solid model of the SENB specimens was generated and.

R3D4 (linear quadrilateral) and C33D8R (linear hexahedral) elements were used to mesh this model. Meshed solid model was given in Fig. 2.7. According to this model, at first maximum displacement obtained from experimental fracture toughness tests was imposed to the material as a boundary condition and elasticity modulus was selected as in the experimental results. After executing the model, maximum force was obtained.

This force was compared with the experimental value and the proportion of them was used to modify the selected elasticity modulus. After modifying the elasticity modulus on Abaqus, the model was run again. This iterative elasticity modulus

Table 2.10 Comparison of the modelling and experimental results for the fracture toughness

Composition name	K_{Ic} FEM (MPa $m^{1/2}$)	Relative difference with experiments
CJ I	0.70	37%
CJ II	0.40	34%
CJ III	0.54	43%

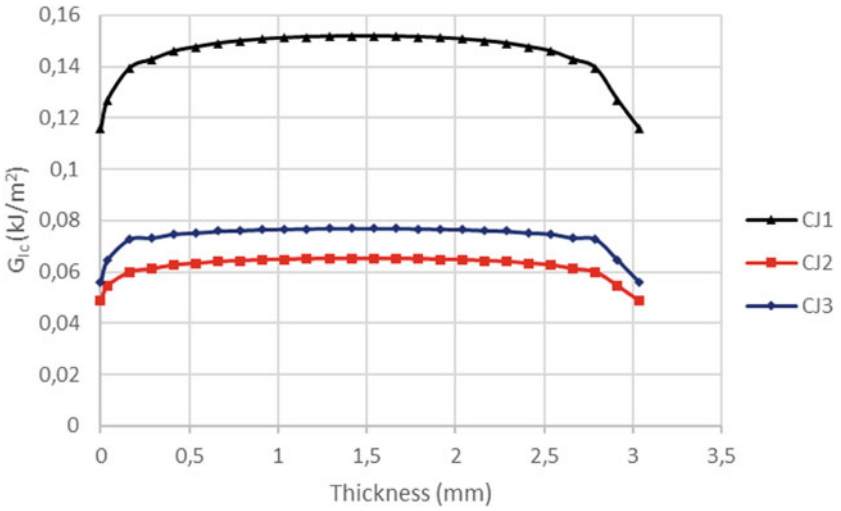

Fig. 2.8 Evolution of G_{Ic} along the specimen thickness according to FEM results

modification continued until obtaining a coherent maximum force value regarding experimental results. After converging to the maximum force, energy releasing rate (G_{ic}) of the composites were determined along the specimen thickness.

From the energy releasing rate results obtained via FEM, Eq. 2.6 can be used to calculate the K_{ic}. After completing the FEM analyses, results were given in Table 2.10.

Finite element results exhibiting significant differences with the experimental results. In fact, inhomogeneity or the existence of hard particles in the crack propagation zone can blunt the cracks. For this reason, experimental results may show a higher trend than modelling. After the comparison of FEM fracture toughness with experimental results, the evolution of the G_{Ic} obtained from FEM is given in Fig. 2.8.

According to Fig. 2.8 strain energy releasing rate have higher values in the middle of the specimen compared to the edges.

As the final step of finite element approach, the real-life conditions of these composites depending on the application area were simulated. As given in the title of this article, these composites are planned to be used in the wing spars of the aircrafts. By considering the airfoil structure and the subjected loads of the wings, the deformation and stress conditions were investigated.

To begin with, in this model, we limited our calculation to a ground situation (static, only the weight of the wing and the fuel tank). Also, the ribs inside the airfoil were not taken into consideration. This FEM approach is implemented to see the mechanical behavior of these composites under static conditions. In this study, NACA (2415) airfoil geometry was used and all parameters required for the FEM analysis were taken as real values of NACA 2415.

After modelling the "I" profile of the wing spar, a distributed load was applied according to Eq. 2.8.

$$q_t(x) = q_w(x) + q_f(x) = \begin{cases} -\frac{W_{Ws}n(C_t x - C_o x + C_o L)}{L^2(C_o + C_t)} - \frac{W_{fs}n(C_{tf}x - C_{of}x + C_{of}L)}{{L_f}^2(C_{of}+C_{tf})} & if\ x \le L_f \\ \frac{n(-\pi C_o L W_{Ws} + \pi C_o W_{Ws} x - \pi C_t W_{Ws} x)}{L^2 \pi (C_o + C_t)} & if\ x \ge L_f \end{cases} \tag{2.8}$$

In this equation, used values are given below in Table 2.11 [7].

By using these values, a distributed load was applied on the wing spar profile as shown in Fig. 2.9. In this wing spar profile, left end of the "I" profile was taken as fixed end to the fuselage.

Table 2.11 Specifications of NACA 2415 airfoil

Total aircraft weight	$W_{to} = 4800$ kg
Weight of wing structure	$W_{Ws} = 630$ kg
Weight of fuel stored in wing	$W_f = 675$ kg
Length of wing	$L = 7$ m
Length of fuel tank within wing	$L_f = 4.8$ m
Chord length at wing root	$C_o = 1.8$ m
Chord length at wing tip	$C_t = 1.4$ m
Width of fuel tank at wing root	$C_{of} = 1.1$ m
Width of fuel tank at *Lf*	$C_{tf} = 0.85$ m
Load factor on the ground	$n = 1$

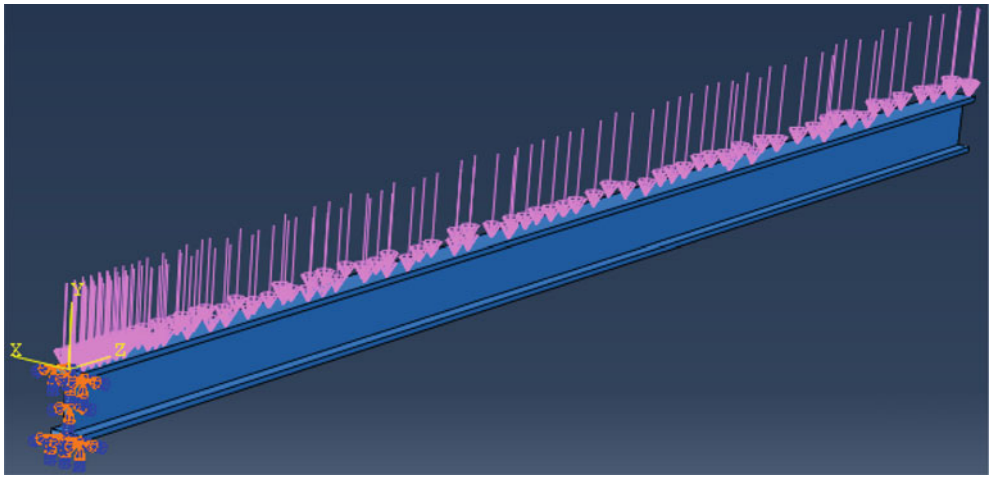

Fig. 2.9 Load profile calculated on the wing spar

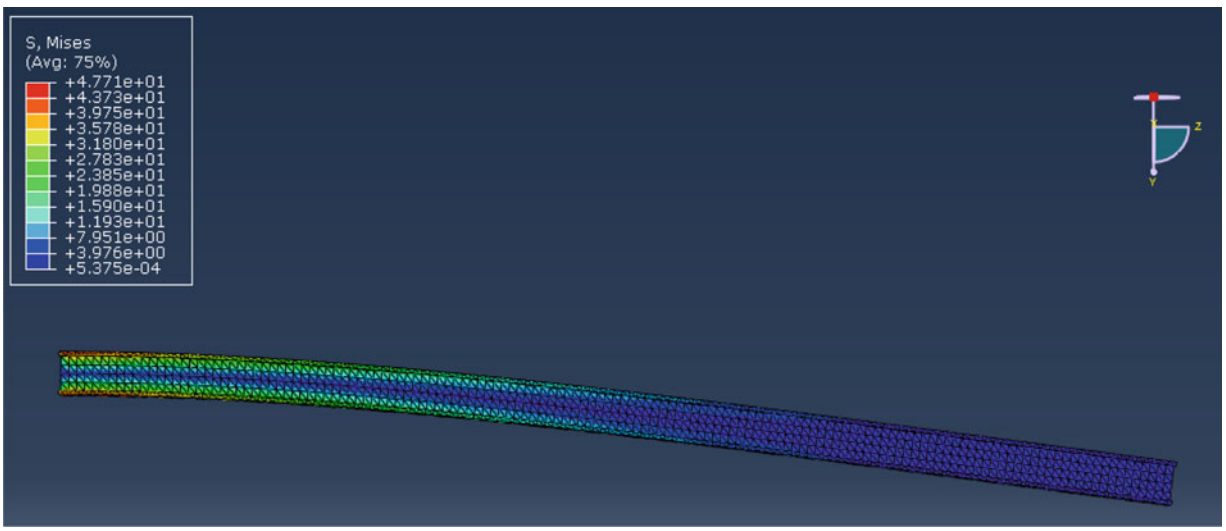

Fig. 2.10 Stress contour on wing spar manufactured by using CJ I composites

After the application of this load profile, wing spar was meshed by using C3D10 (quadratic tetrahedral) elements. Then, this model was executed on Abaqus. The stress contour for a wing spar manufactured by using CJ I composites was presented in Fig. 2.10.

In addition, the results of stress and displacement for the wing spars manufactured by using CJ composites were given in Table 2.12 in detail.

Table 2.12 Stress and displacement results of the modelled wing spar manufactured with CJ composites

Composition	Von Misses (MPa)	σ_{11} (MPa)	σ_{22} (MPa)	σ_{33} (MPa)	U2 (arrow) (m)
CJ I	47.71	21.64	20.36	59.58	1.618
CJ II	47.72	21.41	20.13	59.48	1.532
CJ III	47.72	21.21	20.01	59.17	1.716

These results may seem quite high for the composites in consideration. However, as mentioned before, the real load carrying elements in the airfoils such as aluminum based ribs and the main frame was not considered in this calculation. After integrating these elements to the model, these composites will propose a cost-efficient solution to the aircraft manufacturers.

2.4 Conclusion

In the frame of this research, a new devulcanized rubber based composite reinforced with nano silica + graphene nano plates (GnPs) was developed for the design of wing spar on the aircraft. Comparison of experimental and numerical results have been successfully carried out. Computational techniques were used for the presenting of the various loads acting on the wings of an aircraft; basically the load due to wing structure weight was calculated in Abaqus. Analytical models were also developed and the shear force and bending moments resulting from these loads are also calculated for a small aircraft design. Mechanical behaviour of the real-life application of the composites as aircraft wing spar material was numerically tested. The real load carrying elements in the airfoils such as aluminum based ribs and the main frame was not considered in this stage of the research project that is going on. Next stage of this project, the real load carrying elements in the airfoils will be included in the computational parts.

We believe that this new composite design by using nano silica and graphene nano plates may exposed a novel interface design approach for developing multifunctional rubber based composites in order to manufacture of aircraft wing spar in safety conditions.

Acknowledgments The authors thank Dr. H-A. ALHAS from Airbus-Space, London/UK for general support and also for his valuable discussion in certain stages of this project. Also, they would wish to acknowledge research foundation of Supmeca/Paris.

References

1. Lee, C., Wei, X., Kaysar, J., Hone, J.: Measurement of the elastic properties and intrinsic strength of monolayer graphene. Science. **321**(5887), 385–388 (2008)
2. Oliphant, K., Baker, W.E.: The use of cryogenically ground rubber tires as a filler in polyolefin blends. Polym. Eng. Sci. **33**(3), 166–174 (1993)
3. Naskar, A.K., Bhowmick, A.K., De, S.K.: Thermoplastic elastomeric composition based on ground rubber tire. Polym. Eng. Sci. **41**(6), 1087–1098 (2001)
4. Naskar, A.K., De, S.K., Bhowmick, A.K.: Thermoplastic elastomeric composition based on maleic anhydride–grafted ground rubber tire. J. Appl. Polym. Sci. **84**(2), 370–378 (2002)
5. De Sousa, F.D.B., et al.: Devulcanization of waste tire rubber by microwaves. Polym. Degrad. Stab. **138**, 169–181 (2017)
6. Taheri-Behrooz, F., Shokrieh, M., Abdolvand, H.: Designing and manufacturing of a drop weight impact test machine. Eng. Solid Mech. **1**, 69–76 (2013)
7. Akindapo, J.-O., Johnson Anamemena, N., Garba, D.-K.: Graphite-epoxy composite design for aircraft wing spar using computational techniques – Part I. Am. J. Mech. Eng. **5**(4), 117–127 (2017)
8. D. Zaimova, E. Bayraktar, I. Miskioglu.: Design and manufacturing of new elastomeric composites: Mechanical properties, chemical and physical analysis. Int J Composites Part B, Elsevier, USA. **1**(1), 1–12, November 2016, on line 2017
9. McCarthy, D.W., Mark, J.E., Schaeffer, D.W.: Synthesis, structure, and properties of hybrid organic-inorganic composites based on polysiloxanes. I. Poly (dimethyl siloxanes) elastomers containing silica. J. Polym. Sci. Part B Polym. Phys. **36**, 1167–1189 (1998)
10. Zaimova, D., Bayraktar, E., Miskioglu, I., Dishovsky, N.: Wear resistance of elastomeric based composites by continuous multicycle indentation used in manufacturing engineering. Adv. Mater. Res. **939**, 106–113 (2014), Trans Tech Publications, Switzerland, Doi:10.4028/www.scientific.net/AMR.939.106
11. Sadasivuni, K.-K., Ponnamma, D., Thomas, S., Grohens, Y.: Evolution from to graphene elastomer composites. Prog. Polym. Sci. **39**, 749–778 (2014)
12. Irez, A. B., Bayraktar, E., Miskioglu, I.: Mechanical Characterization of Epoxy – Scrap Rubber Based Composites Reinforced With Alumina Fibers, Springer link, Mechanics of Composite and Multi-functional Materials, vol 6, pp. 59–70 (2017), ISBN 978-3-319-63408-1, https://doi.org/10.1007/978-3-319-63408-1